Identification of Interplanetary Parameter Schemes which Drive the Variability of the Magnetospheric Radiation Environment

Ch. Katsavrias [1,2,3], A. Nasi[1,2], C. Papadimitriou[2], S. Aminalragia-Giamini[2], I. Sandberg[2], P. Jiggens[4], I. A. Daglis[1,3,5] and H. Evans[4]

1. Department of Physics, National and Kapodistrian University of Athens, Greece.
2. Space Applications and Research Consultancy (SPARC), Athens, Greece
3. Institute of Accelerating Systems and Applications, National and Kapodistrian University of Athens, Greece.
4. ESA/ESTEC, Netherlands.
5. Hellenic Space Center, Athens, Greece.

EGU General Assembly, May 2020, Vienna, Austria.

Motivation

1. Identify Solar, Solar wind and geomagnetic parameters that drive the variability of the radiation environment

2. Identify Solar cycle variations

Data & Analysis

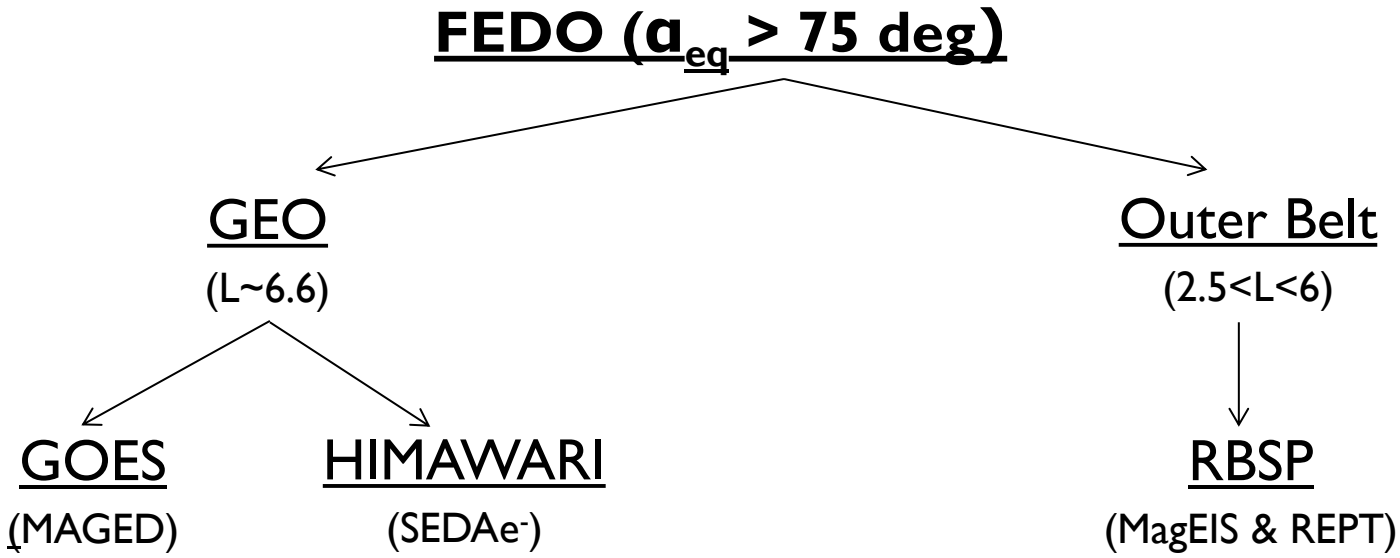

Time: 1/2011 – 7/2019
Energy: 30 – 1500 keV

Time: 9/2012 – 7/2019
Energy: 30 – 9900 keV

Data & Analysis

OMNIWeb

- Interplanetary Magnetic Field (IMF) and Bx, By and Bz component in GSM coordinates and nT.
- Azimuthal electric field (Ey = -Vsw*BzGSM*10^{-3}) in mV/m and Bs (the difference between Ey and Bs is that for the calculation of the latter all positive Bz values are set to zero).
- Solar wind speed (Vsw) in km/s and dynamic pressure (Psw) in nPa.
- Proton density (Np) in particles/cm^3 and temperature (Tp) in K.
- Solar wind Plasma beta and Alfven Mach number
- Kp, Ap, Dst, AE, AL and AU geomagnetic indices.
- Sunspot number (Rz) and Solar flux (f10.7) index.

Data & Analysis

Universal coupling functions

- Southward magnetic field [Bs = Bz(Bz≤0)]
- Half-Wave Rectifier [$HWR = VSW \cdot BS$] (corresponds to the rate of reconnection)
- Epsilon [$\varepsilon = V_{SW} \cdot \mathrm{B}^2 \cdot \sin^4\left(\frac{\theta}{2}\right)$] (epsilon describes the Poynting flux incident at the magnetopause *[Akasofu, 1981]*)
- $\frac{d\varphi}{dt} = {V_{SW}}^{4/3} \cdot {\mathrm{B}_{TAN}}^{2/3} \cdot \sin^{8/3}\left(\frac{\theta}{2}\right)$ (the universal coupling function s proportional to the rate at which magnetic flux is opened at the magnetopause *[Newell et al., 2007]*)
- $\boldsymbol{E_{WAV}} = V_{SW} \cdot \mathrm{B_{TAN}} \cdot \sin^4\left(\frac{\theta}{2}\right)$ *[Wygant et al., 1983]*
- $\boldsymbol{E_{KL}} = VSW \cdot \mathrm{B_{TAN}} \cdot \sin^2\left(\frac{\theta}{2}\right)$ *[from Kan and Lee, 1979]*

Data & Analysis

- **3 different binnings**:
  - annual,
  - monthly
  - daily

- For each type of binning a full distribution is provided (mean, std, median, quantiles)

- For each component of the distribution we calculate:
  - Pearson's product moment correlation coefficient
  - Spearman's rank-order correlation coefficient

GEO results

CCs vs Energy

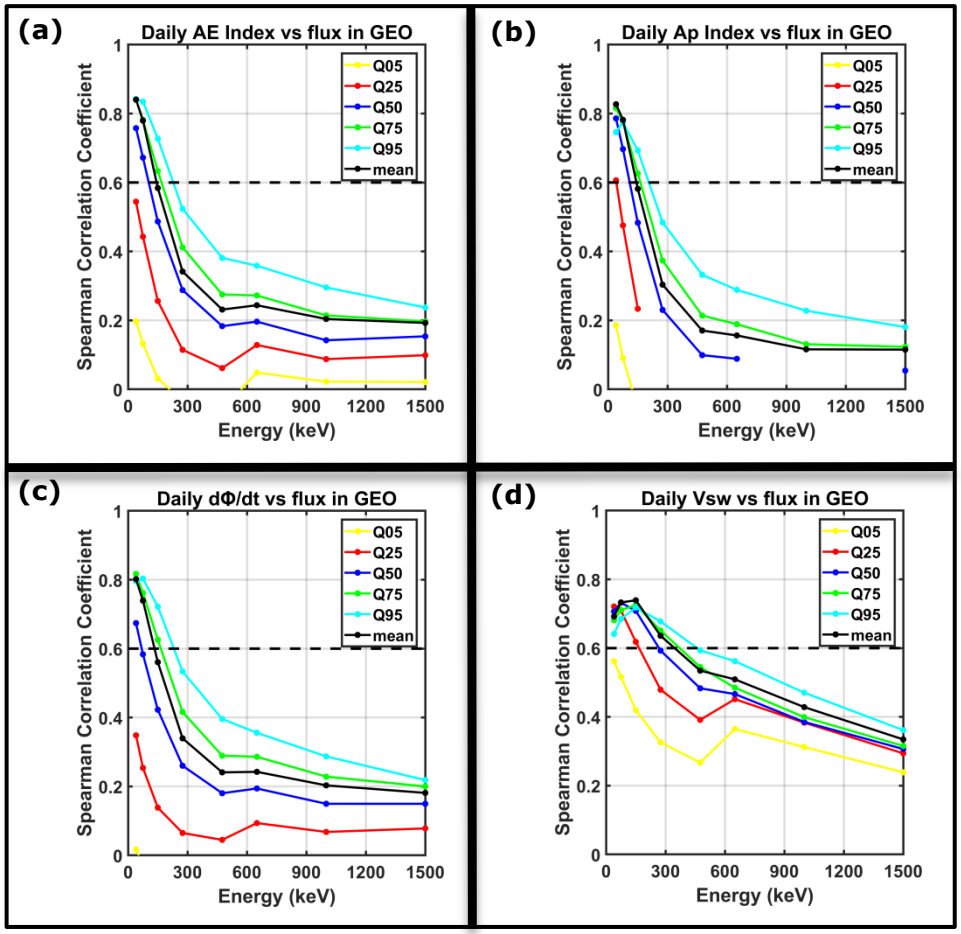

GEO results

CCs vs Energy

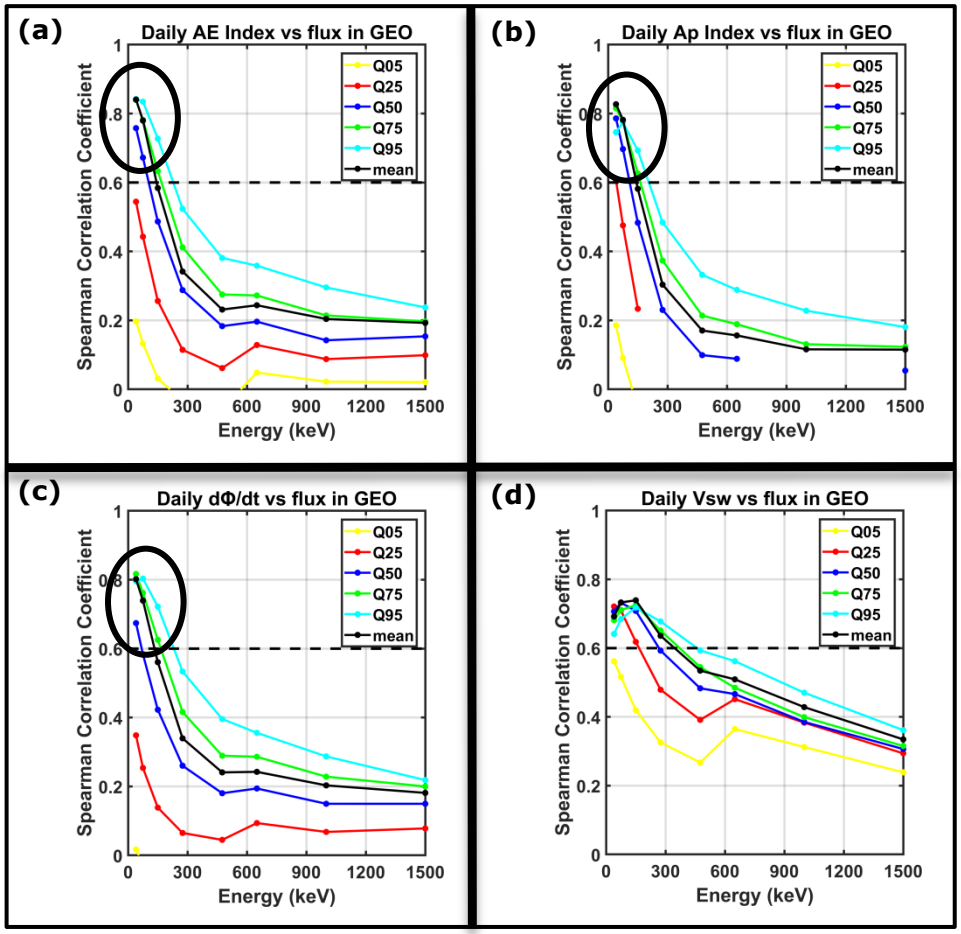

Strong correlation of the lower energy channels of GOES (40 and 75 keV) with the AE and AP index along with the Newell function especially concerning Q50, Q75, Q95 and the mean which clearly indicates the relationship between substorm activity and source electron flux at GEO.

GEO results

CCs vs Energy

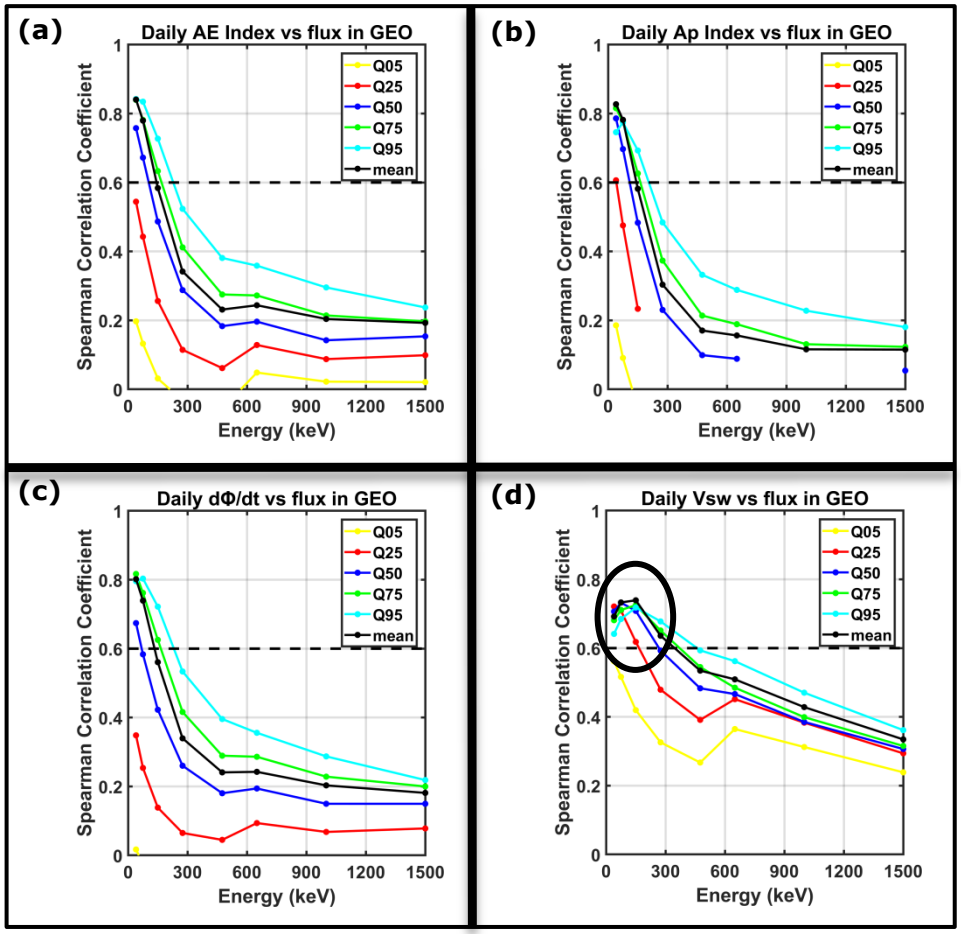

Strong correlation of the 150 and 275 keV electron flux with the solar wind speed.

GEO results

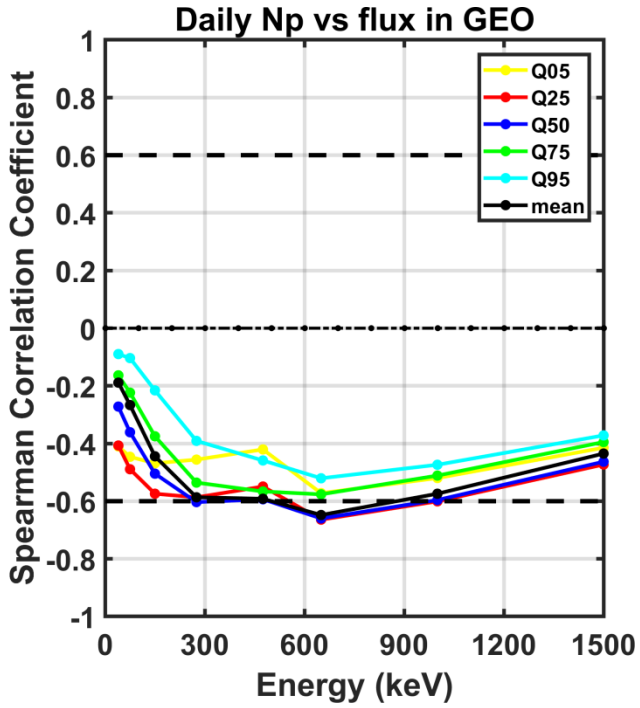

Strong anti-correlation of the lower energy channels of ~ 600 keV with density.

Nevertheless, this result is based on HIMAWARI data which have much less time-span.

GEO results

CC vs Year for 40 keV

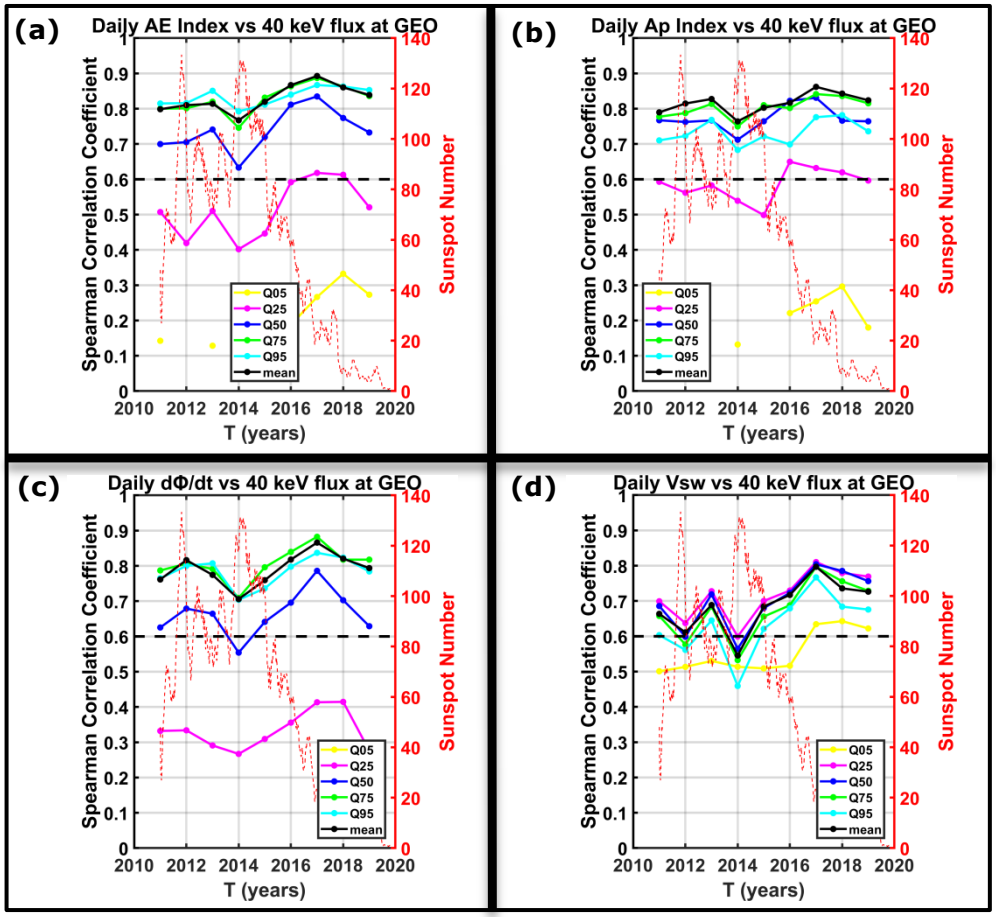

There is a clear dependence (anti-correlation) on solar cycle phase between the CCs of 40 keV flux and AE index and solar wind speed.

Their minimum is during 2014 (SC maximum) and their maximum during 2017 (SC declining phase).

GEO results

CC vs Year for 275 keV

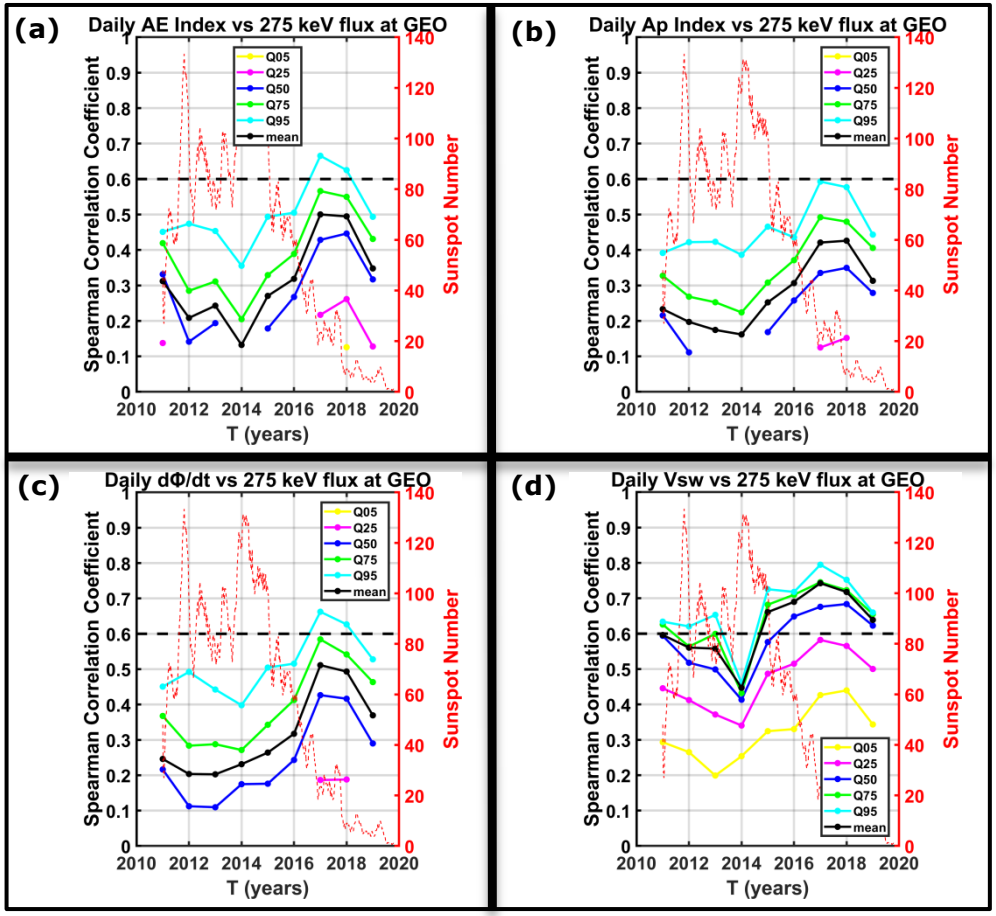

This anti-correlation is exhibited by all GOES channels.

Yet solar wind speed becomes more important for electrons higher than 150 keV.

GEO results

CC vs Year for Np

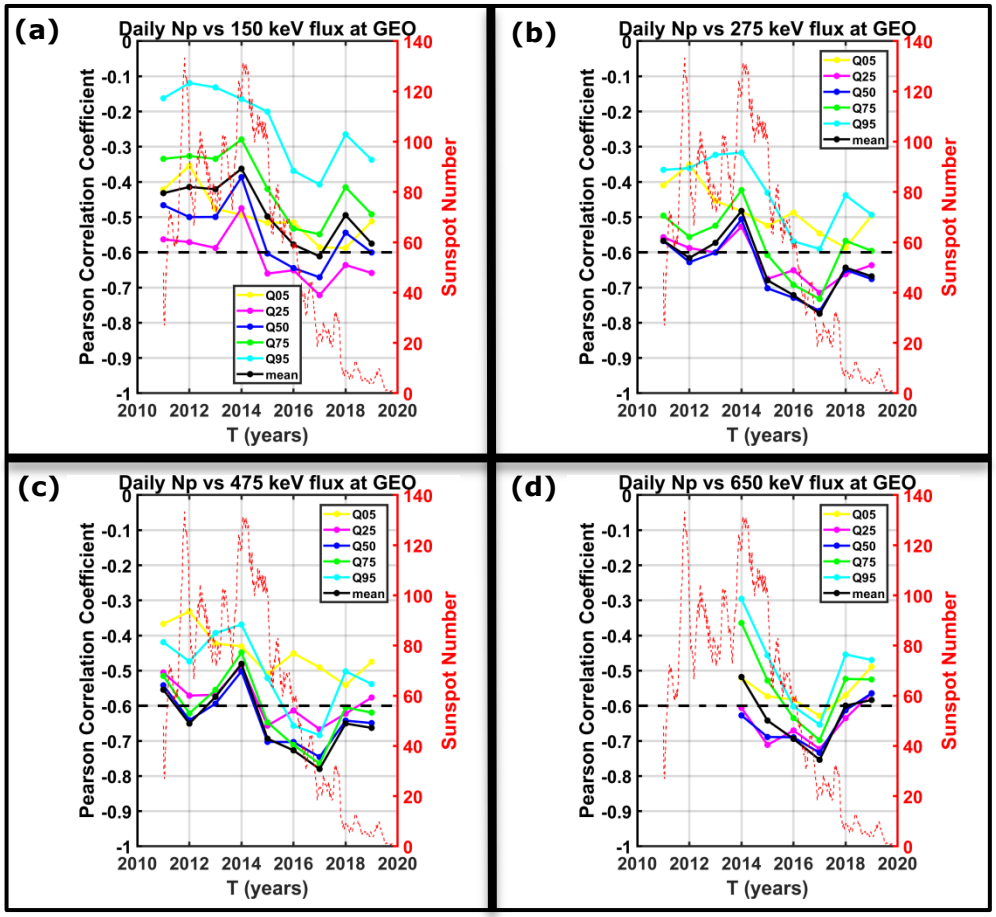

Outer Belt results

CCs vs Energy

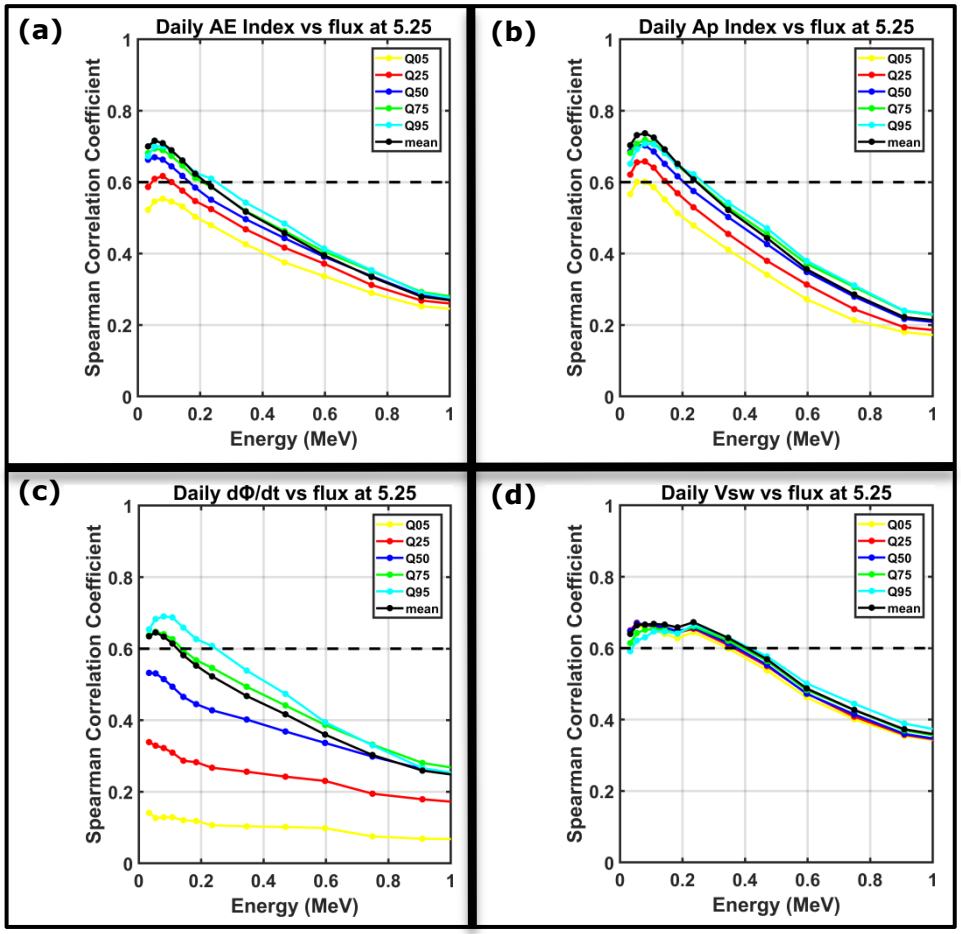

Strong correlation of the lower energy channels of MagEIS (especially 54 and 80 keV) with the AE and AP index along with the Newell function especially concerning Q50, Q75, Q95 and the mean which clearly indicates the relationship between substorm activity and source electron flux at GEO.

Strong correlation of the >200 keV electron flux with the solar wind speed.

Outer Belt results

CCs vs L for 80 keV

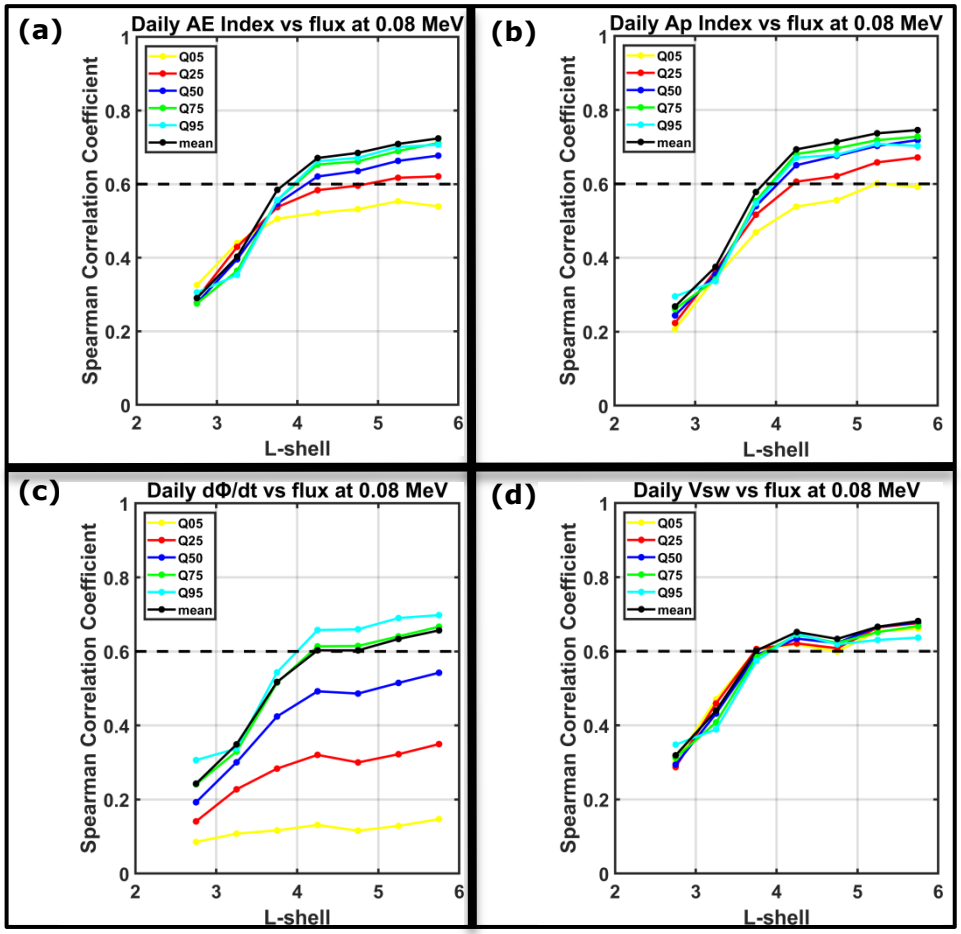

CCs are L-dependent as they increase with increasing L-shell.

Generally, we accept CCs down to L=4.

Outer Belt results

CCs vs Year for 80 keV

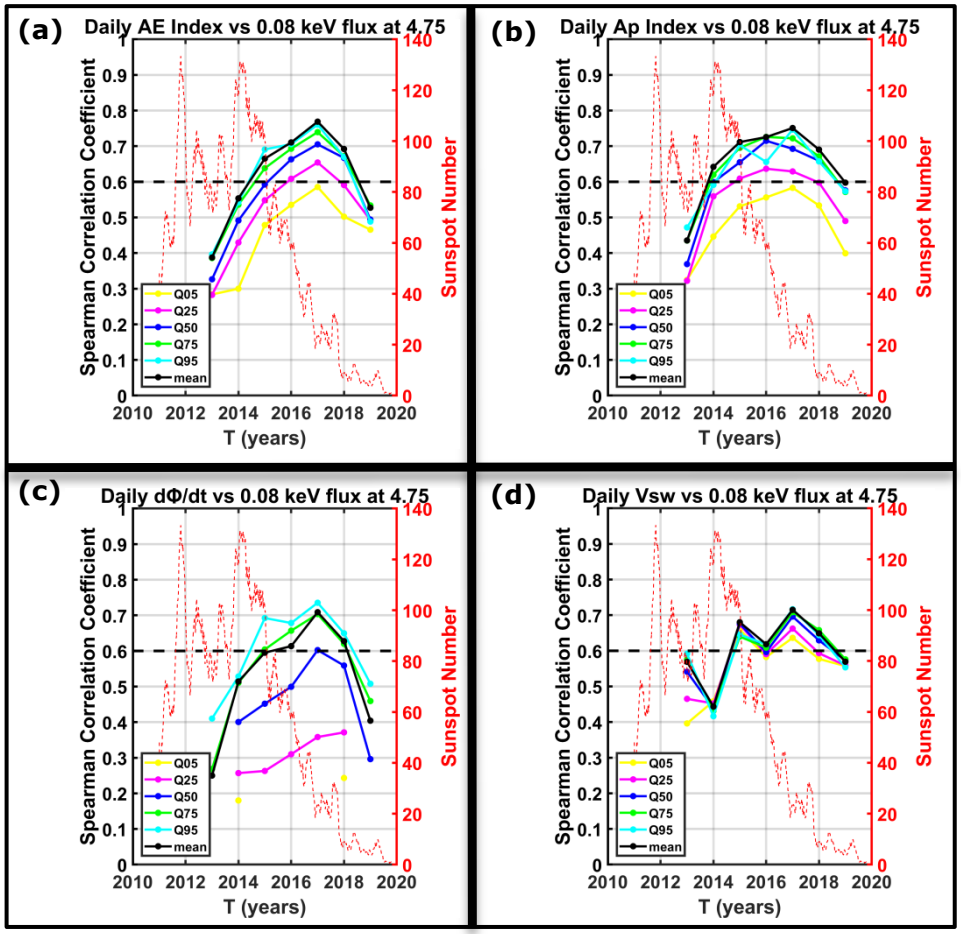

There is a clear dependence (anti-correlation) on solar cycle phase between the CCs of 80 keV flux and AE index and solar wind speed.

Their minimum is during 2013 (SC maximum) and their maximum during 2017 (SC declining phase).

Multiple Regression Model

General form:

$$log(J) = a_0 + a_1 \cdot X_1 + a_2 \cdot X_2 + a_3 \cdot X_3 + a_4 \cdot X_4 + a_5 \cdot {X_1}^2 + a_6 \cdot {X_2}^2 + a_7 \cdot {X_3}^2 + a_8 \cdot {X_4}^2$$

where

$X_1 = log(P_{SW})$, $X_2 = log(B_S)$, $X_1 = log(V_{SW})$ and $X_1 = log(IMF)$

Multiple Regression Model

Daily MLT averaged flux at 40 keV

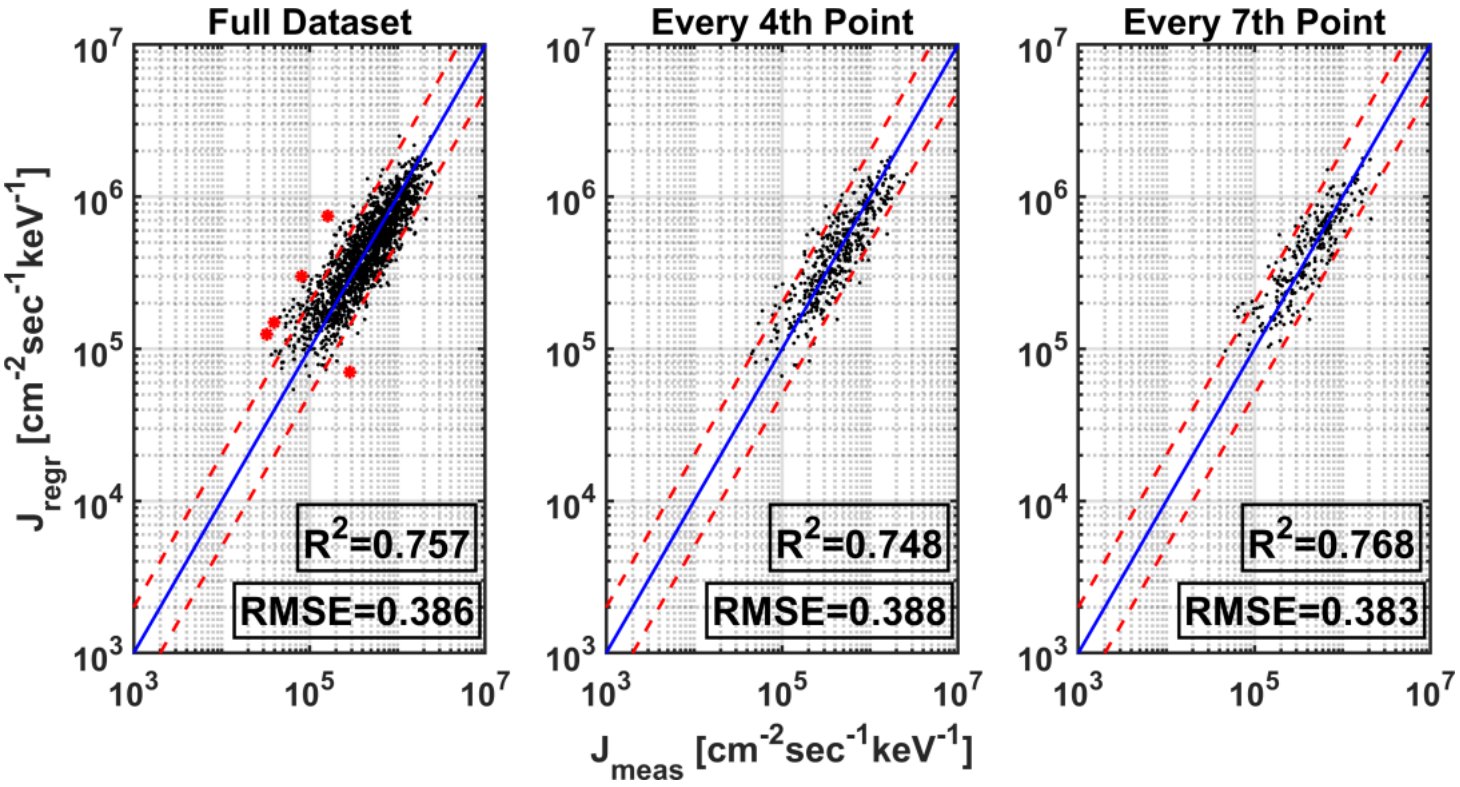

a_0	a_1	a_2	a_3	a_4	a_5	a_6	a_7	a_8
-54,17	0,34	0,21	19,16	1,07	-0,2	0,006	-1,36	-0,21

Multiple Regression Model

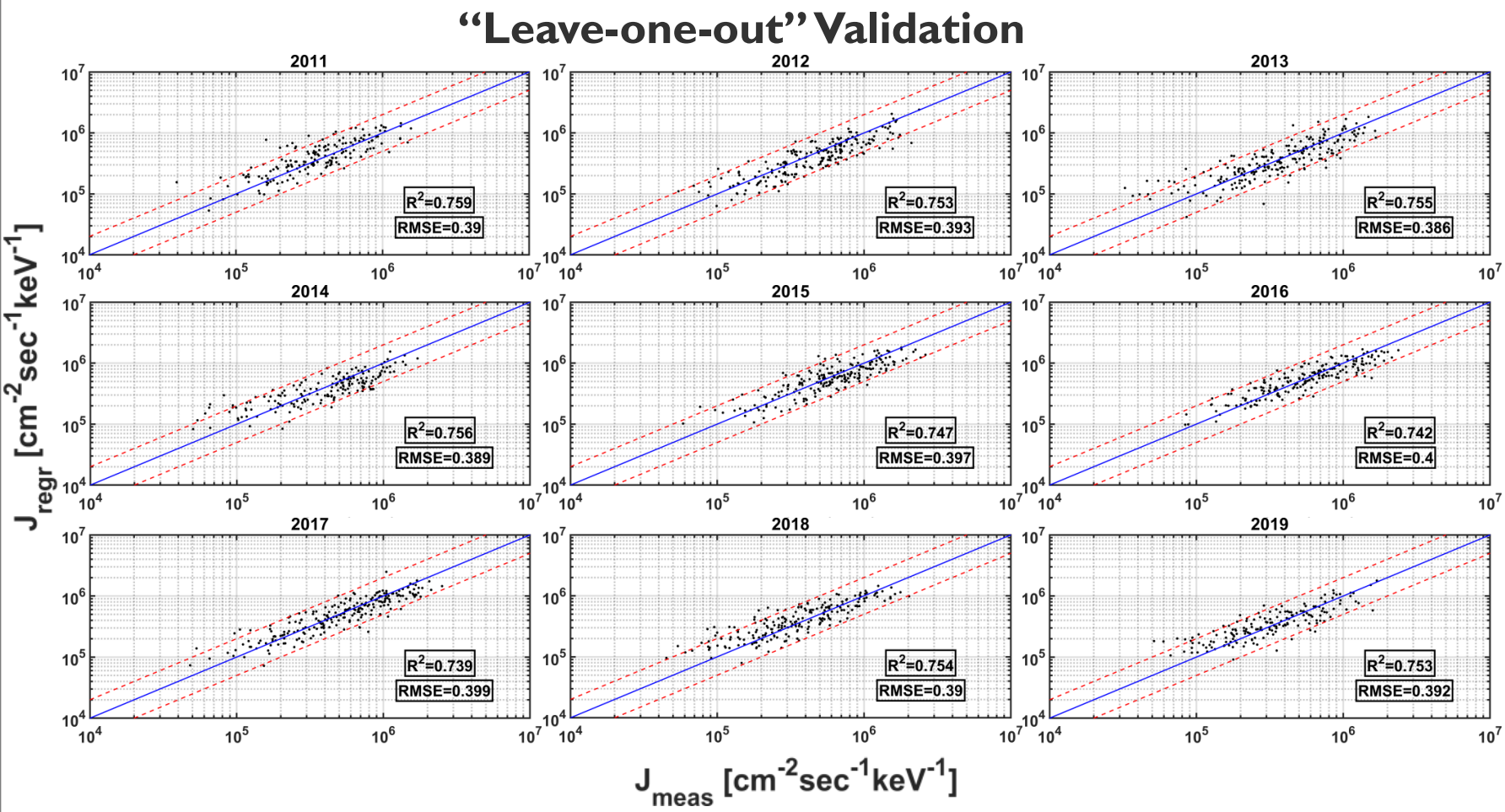

The daily distribution of flux during the year whose distribution is to be predicted is not taken into account.

Multiple Regression Model

"Leave-one-out" Validation

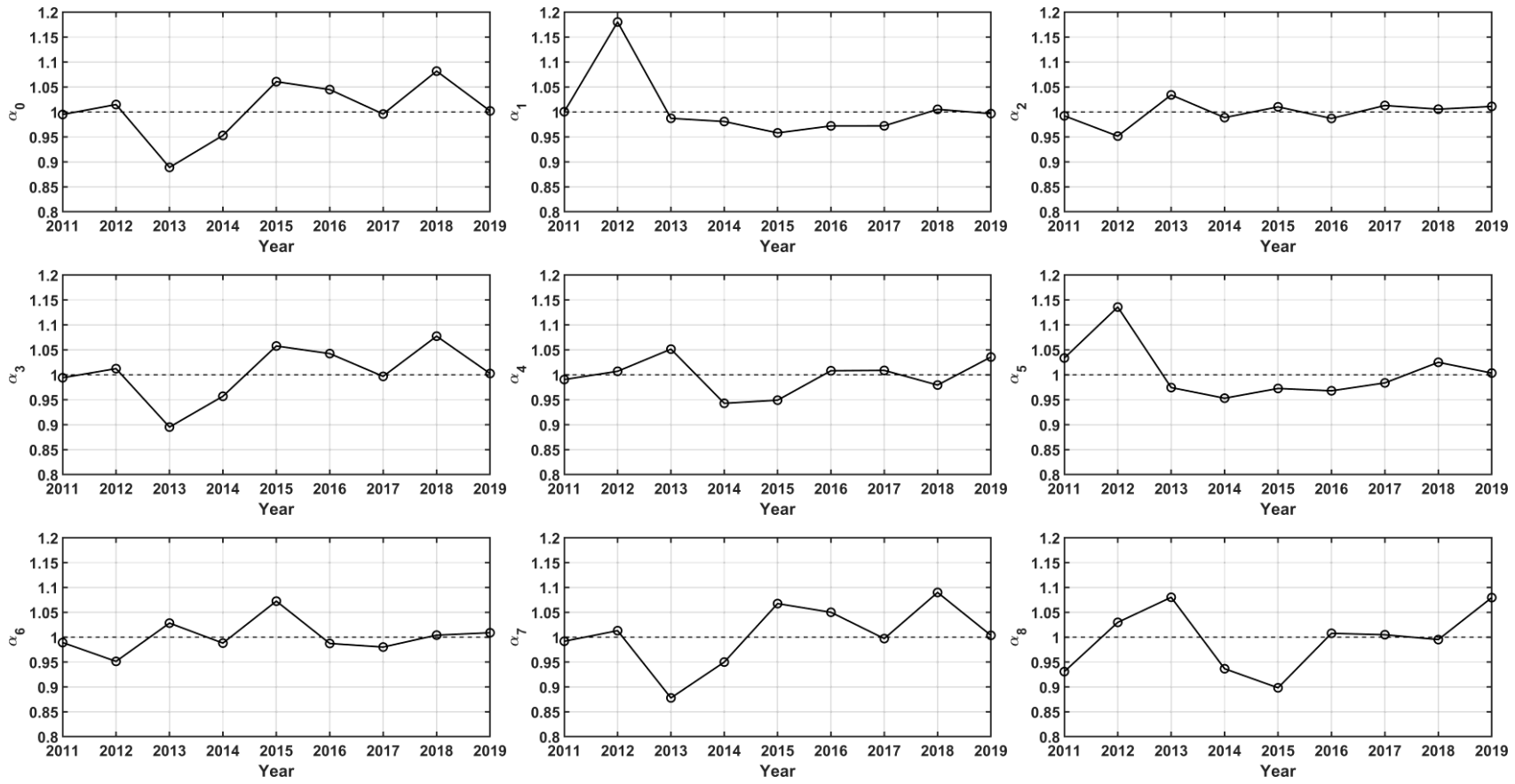

Ratio of the parameters calculated using the "leave-one-out" validation over the free parameters of the full dataset

Multiple Regression Model

Comparison with 5-min flux from GOES during the St. Patrick's 2015 storm

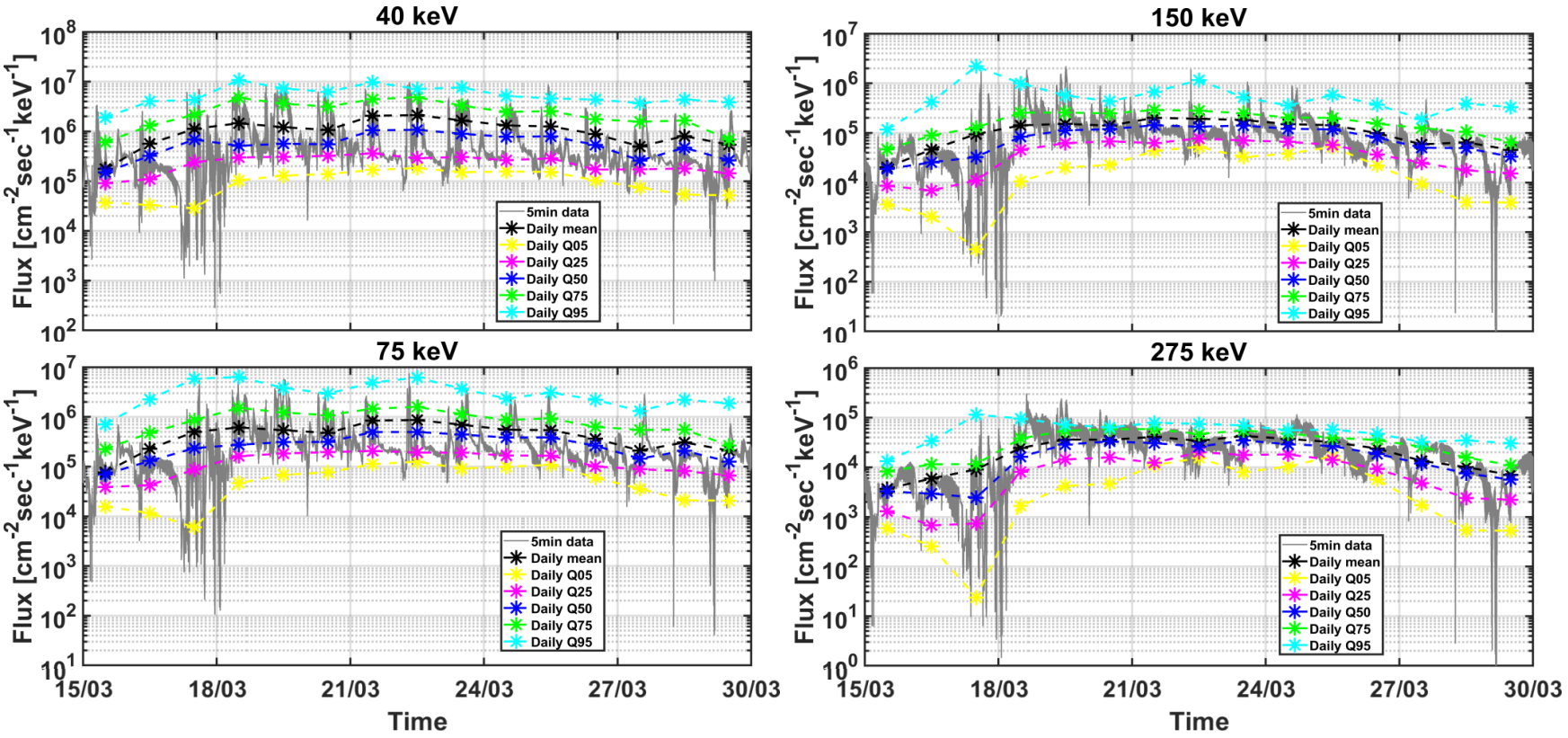

Multiple Regression Model

Comparison with 5-min flux from GOES during the April 2017 storm

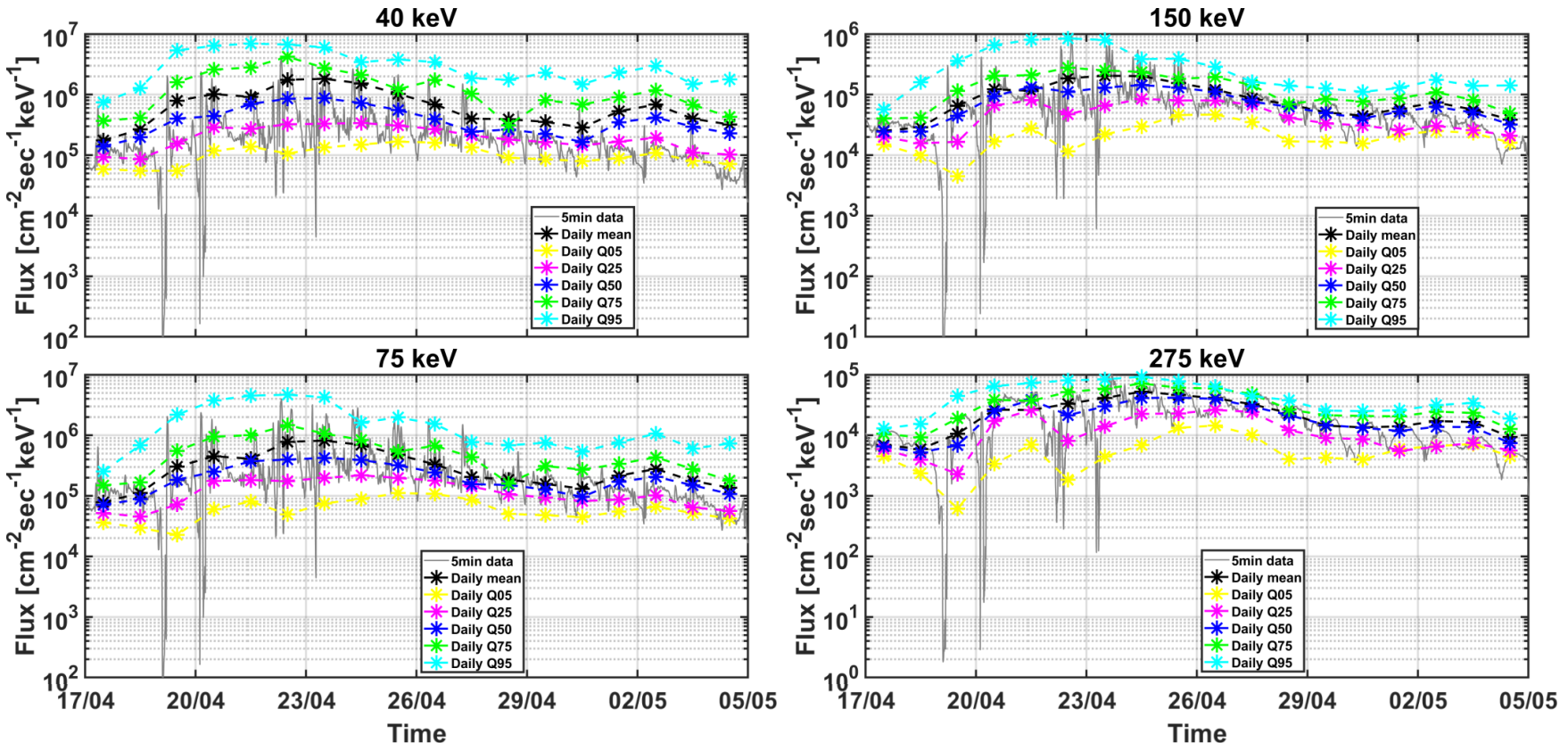

Conclusions

- Source electron (10--100 keV) fluxes at GEO are dominantly driven by substorm activity (in terms of AE index) while, seed electron (100--350 keV) fluxes are mostly driven by solar wind speed..
- CCs are highly anti--correlated with the SC24 phase which is translated as a strong indication that source/seed electron fluxes at GEO are dominantly driven by high speed streams..
- CCs remain higher than 0.6 for L-shells down to 4.
- The developed regression model can successfully predict the daily distribution of source/seed electron fluxes in the 30--350 keV energy range.
- The model may have a variety of applications related to nowcasting/forecasting of the distribution of electron fluxes at GEO (e.g. serve as low-energy boundary conditions for studying electron acceleration to relativistic energies or provide information for predicting surface charging effects on spacecraft).

Thank you
for your Attention

Backup Slides

GEO results

CCs Distribution

DAILY Q50	IMF	B_X	B_Y	B_Z	B_{TAN}	E_Y	V_{SW}	P_{SW}	T	N	Plasma β	M_{Alfven}	Dst	AE	AU	AL	Ap	Kp	Rz	Flux 10.7	E_{WAV}	ε	Bs	E_{KL}	HWR	dφ/dt
40 keV	0,289	NaN	NaN	-0,404	0,175	0,427	0,706	0,327	0,618	-0,272	-0,156	-0,376	-0,762	0,758	0,705	0,772	0,786	0,789	0,058	0,061	0,134	0,619	-0,411	0,257	0,459	0,674
75 keV	0,202	NaN	NaN	-0,323	0,083	0,348	0,732	0,245	0,603	-0,361	-0,114	-0,357	-0,742	0,672	0,607	0,688	0,697	0,7	NaN	0,038	0,104	0,515	-0,326	0,21	0,377	0,583
150 keV	NaN	NaN	NaN	-0,222	-0,122	0,247	0,708	0,058	0,518	-0,505	NaN	-0,276	-0,668	0,487	0,395	0,507	0,483	0,486	NaN	NaN	0,053	0,327	-0,208	0,102	0,259	0,423
275 keV	-0,223	NaN	NaN	-0,16	-0,329	0,183	0,593	-0,159	0,351	-0,603	0,115	-0,156	-0,52	0,288	0,194	0,312	0,23	0,233	-0,086	-0,09	NaN	0,134	-0,123	NaN	0,166	0,26
475 keV	-0,322	NaN	NaN	-0,145	-0,408	0,164	0,483	-0,248	0,234	-0,593	0,178	-0,076	-0,4	0,183	0,105	0,207	0,099	0,101	-0,105	-0,116	-0,045	0,044	-0,096	-0,095	0,131	0,18

DAILY Q75	IMF	B_X	B_Y	B_Z	B_{TAN}	E_Y	V_{SW}	P_{SW}	T	N	Plasma β	M_{Alfven}	Dst	AE	AU	AL	Ap	Kp	Rz	Flux 10.7	E_{WAV}	ε	Bs	E_{KL}	HWR	dφ/dt
40 keV	0,349	NaN	0,099	-0,28	0,276	0,646	0,681	0,384	0,632	-0,164	-0,189	-0,37	-0,651	0,84	0,765	0,716	0,816	0,819	0,043	0,048	0,3	0,721	-0,283	0,407	0,649	0,817
75 keV	0,301	0,037	0,07	-0,249	0,221	0,577	0,711	0,338	0,631	-0,224	-0,177	-0,375	-0,671	0,781	0,705	0,685	0,776	0,779	NaN	0,038	0,274	0,653	-0,24	0,375	0,58	0,762
150 keV	0,138	NaN	NaN	-0,25	0,051	0,436	0,725	0,18	0,571	-0,375	-0,124	-0,356	-0,699	0,633	0,55	0,601	0,626	0,629	NaN	NaN	0,205	0,486	-0,186	0,276	0,439	0,625
275 keV	-0,12	NaN	-0,05	-0,289	-0,197	0,264	0,651	-0,053	0,414	-0,536	NaN	-0,264	-0,641	0,412	0,328	0,461	0,373	0,376	-0,069	-0,074	0,077	0,237	-0,139	0,098	0,264	0,416
475 keV	-0,255	NaN	-0,085	-0,316	-0,319	0,18	0,545	-0,168	0,284	-0,566	0,066	-0,182	-0,543	0,275	0,2	0,358	0,214	0,216	-0,098	-0,109	NaN	0,099	-0,123	NaN	0,178	0,289

DAILY Q95	IMF	B_X	B_Y	B_Z	B_{TAN}	E_Y	V_{SW}	P_{SW}	T	N	Plasma β	M_{Alfven}	Dst	AE	AU	AL	Ap	Kp	Rz	Flux 10.7	E_{WAV}	ε	Bs	E_{KL}	HWR	dφ/dt
40 keV	0,346	0,094	0,182	-0,04	0,301	0,702	0,641	0,365	0,608	-0,09	-0,169	-0,3	-0,482	0,842	0,713	0,481	0,746	0,746	NaN	NaN	0,45	0,653	-0,123	0,487	0,702	0,796
75 keV	0,355	0,126	0,164	NaN	0,306	0,689	0,685	0,377	0,634	-0,104	-0,169	-0,313	-0,502	0,834	0,7	0,487	0,774	0,774	NaN	NaN	0,461	0,655	-0,108	0,501	0,689	0,803
150 keV	0,254	0,1	0,104	-0,069	0,201	0,57	0,718	0,275	0,603	-0,216	-0,175	-0,342	-0,573	0,727	0,597	0,488	0,693	0,693	NaN	NaN	0,402	0,546	-0,088	0,435	0,57	0,722
275 keV	NaN	NaN	NaN	-0,217	NaN	0,36	0,678	0,061	0,467	-0,391	-0,133	-0,324	-0,617	0,524	0,412	0,46	0,484	0,484	-0,048	-0,05	0,24	0,314	-0,074	0,256	0,36	0,534
475 keV	-0,123	-0,042	-0,093	-0,304	-0,167	0,232	0,593	-0,063	0,345	-0,459	-0,078	-0,273	-0,585	0,381	0,286	0,407	0,332	0,332	-0,08	-0,087	0,119	0,161	-0,067	0,123	0,232	0,396